Supplementary Material of Enhanced Sparse Model for Blind Deblurring

Liang Chen[1], Faming Fang[1] *, Shen Lei[2], Fang Li[3], and Guixu Zhang[1]

[1] Shanghai Key Laboratory of Multidimensional Information Processing, School of Computer Science and Technology, East China Normal University
[2] School of Software Engineering, East China Normal University
[3] School of Mathematical Sciences, East China Normal University
{ liangchen527, lstresa}@gmail.com, {fmfang, gxzhang}@cs.ecnu.edu.cn, fli@math.ecnu.edu.cn

In this supplementary file, we provide,
1. Detail description for the solution of Eq. (5) in the paper.
2. Effectiveness of the proposed noise modelling step.
3. More comparison results with other state-of-the-art methods.

1 Proof of our solution for Eq. (5) in the paper

Eq. (5) in the manuscript is given by,

$$\min_{\mathcal{B}_i} \frac{1}{4\sigma^2} \sum_i |\mathcal{A}_i - \mathcal{B}_i|^2 + |\mathcal{B}_i|^e, \tag{1}$$

and the solution can be written as,

$$\mathcal{B}_i = \begin{cases} \mathcal{A}_i + 2\sigma^2, & \text{if } \ \mathcal{A}_i + 2\sigma^2 < -2\sigma \\ \mathcal{A}_i - 2\sigma^2, & \text{if } \ \mathcal{A}_i - 2\sigma^2 > 2\sigma \\ 0, & \text{Otherwise.} \end{cases} \tag{2}$$

Proof. Denoting by $\mathcal{E}$ the energy of Equation (1). Referring to our definition of l_e norm, we rewrite Equation (1) as follow,

$$\mathcal{E}(\mathcal{B}_i) = \min_{\mathcal{B}_i} |\mathcal{B}_i|^0 + |\mathcal{B}_i| + \frac{1}{4\sigma^2}|\mathcal{A}_i - \mathcal{B}_i|^2. \tag{3}$$

1) When $\mathcal{B}_i = 0$,

$$\mathcal{E}(0) = \frac{(\mathcal{A}_i)^2}{4\sigma^2}. \tag{4}$$

2) When $\mathcal{B}_i \neq 0$,

$$\arg\min_{\mathcal{B}_i} \mathcal{E}(\mathcal{B}_i) = \arg\min_{\mathcal{B}_i} |\mathcal{B}_i| + \frac{1}{4\sigma^2}|\mathcal{A}_i - \mathcal{B}_i|^2, \tag{5}$$

* Corresponding Author

which is an one-dimension shrinkage formulation. In this case,

$$\mathcal{E}(\mathcal{B}_i) = \begin{cases} 1 - \mathcal{A}_i - \sigma^2, & \mathcal{B}_i = \mathcal{A}_i + 2\sigma^2 < 0 \\ 1 + \mathcal{A}_i - \sigma^2, & \mathcal{B}_i = \mathcal{A}_i - 2\sigma^2 > 0. \end{cases} \tag{6}$$

When $\mathcal{B}_i$ takes the value of $\mathcal{A}_i + 2\sigma^2$, which implies $\mathcal{E}(\mathcal{B}_i) < \mathcal{E}(0)$. In this case, we have $\mathcal{A}_i + 2\sigma^2 < -2\sigma$. Similar for another condition. Thus, combining above cases, we can easily have the optimal solution of $\mathcal{B}_i$ in Equation (2).

Compared with the case when minimizing l_0 model, which has the solution of $\mathcal{B}_i = \mathcal{A}_i$ if $(\mathcal{A}_i)^2 \geq 4\sigma^2$, or $\mathcal{B}_i = 0$ if $(\mathcal{A}_i)^2 < 4\sigma^2$, the solutions are more likely to be 0 given the same settings (i.e. σ and $\mathcal{A}_i$). This explains the reason why l_e model is able to achieve sparser solutions than that of l_0 model.

2 Effectiveness of the noise modelling step

As demonstrated in the manuscript, the noise modeling step is given by,

$$F(y - x \star k) = \|y - x * k\|_2^2 + \beta \|\nabla y - \nabla x * k\|_e. \tag{7}$$

The weight β in the equation plays an important role to balance the two parts, and it is determined by conducting ablation study on dataset [8]. Figure 1 (a) illustrates that when the weight is set in a reasonable range (0.001 - 0.005), the deblurring result can be improved, which demonstrates the effectiveness of the proposed noise modelling step. Moreover, to further validate the noise modeling step, we combine the real-life noise from [17] with the images provided by [8]. The effect of β is shown in Figure 1 (b). The phenomenon demonstrates the fact that our noise modeling step is useful when confronts real noise, and the optimal selection of β also lies in the range form 0.001 to 0.005.

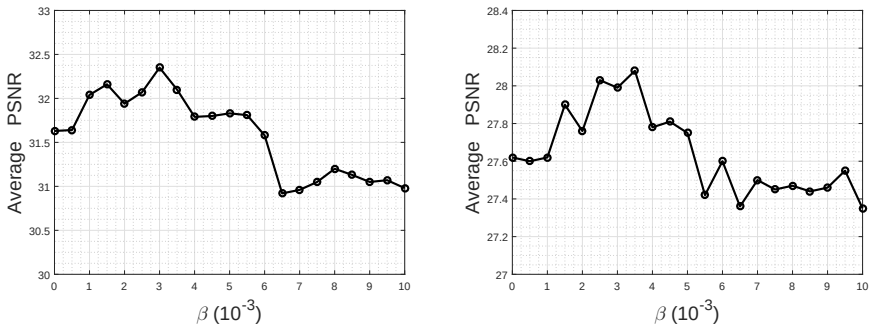

Fig. 1. Effectiveness of the l_e norm on the proposed noise-fitting model. (a) Effect of the weight parameter in (7) on the dataset [8]. (b) Effect of the weight parameter for l_e norm in (7) on the dataset [8] corrupted with real noise provided by [17].

3 More comparison results

In this section, we provide more visual comparisons with state-of-the-art deblurring methods. The codes we used are from author's website, and most parameters are set according to their papers. For fair comparison, we use the same set of parameters for our code both in the paper and the supplementary material.

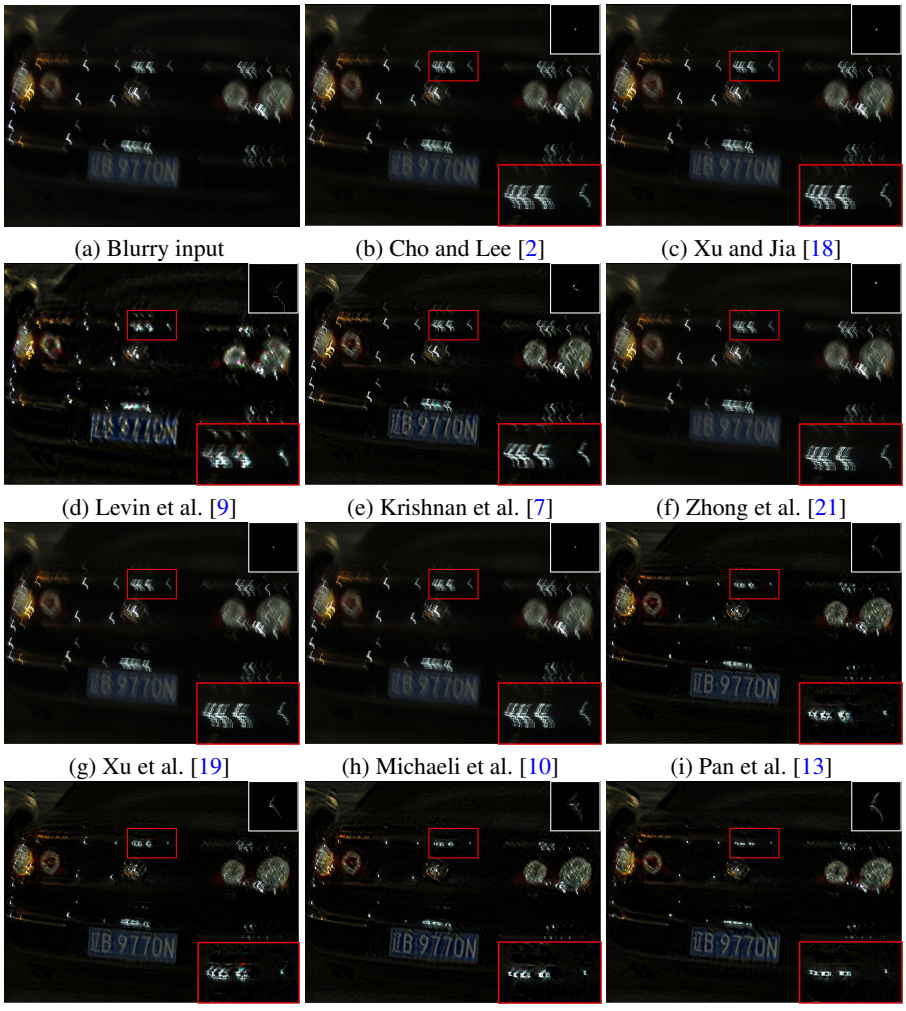

(a) Blurry input (b) Cho and Lee [2] (c) Xu and Jia [18]

(d) Levin et al. [9] (e) Krishnan et al. [7] (f) Zhong et al. [21]

(g) Xu et al. [19] (h) Michaeli et al. [10] (i) Pan et al. [13]

(o) Yan et al. [20] (p) Chen et al. [1] (q) Ours

Fig. 2. Comparisons with state-of-the-art deblurring methods using real-world blur image. Here we use the same non-blid deconvolution method from [16] after the kernels are obtained. Our method generates clearer image than the sate-of-the-art methods.

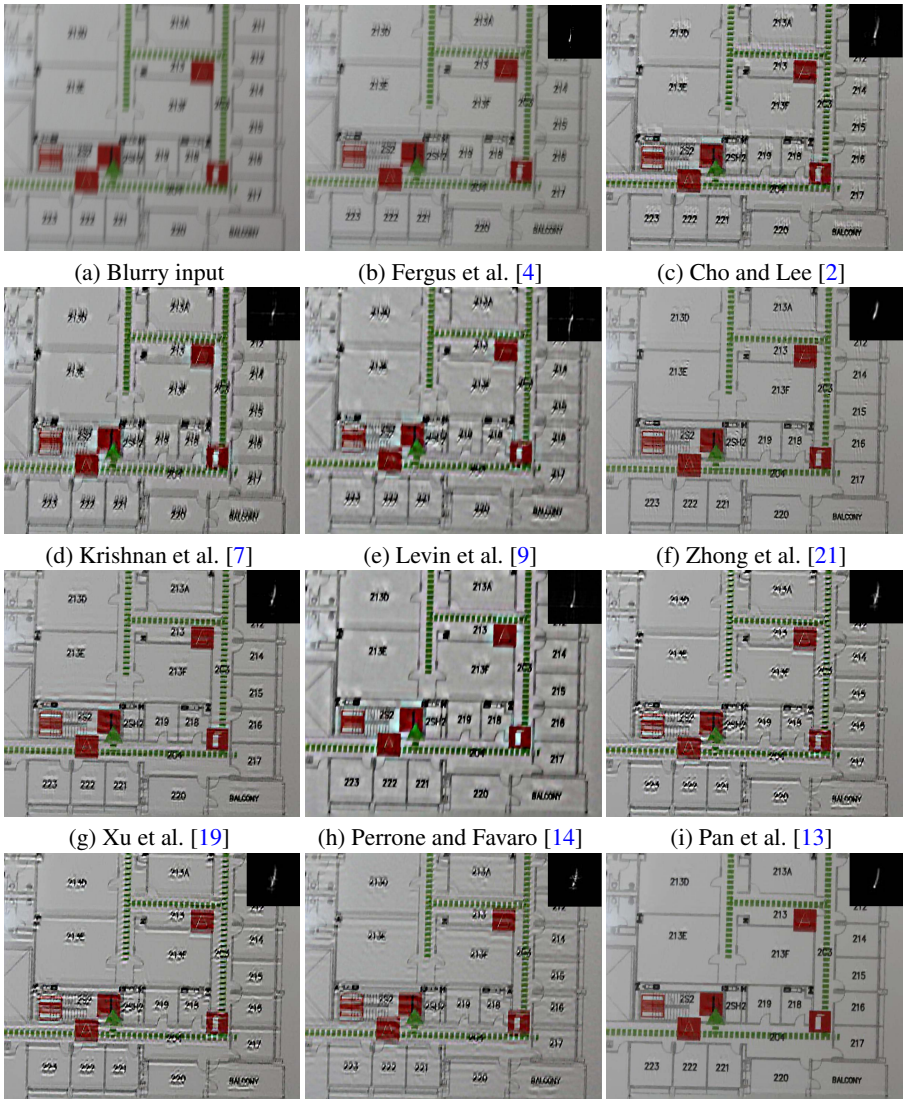

(a) Blurry input (b) Fergus et al. [4] (c) Cho and Lee [2]

(d) Krishnan et al. [7] (e) Levin et al. [9] (f) Zhong et al. [21]

(g) Xu et al. [19] (h) Perrone and Favaro [14] (i) Pan et al. [13]

(j) Yan et al. [20] (k) Chen et al. [1] (l) Ours

Fig. 3. Comparisons with state-of-the-art deblurring methods using real-world blur image. Here we use the same non-blid deconvolution method from [12] after the kernels are obtained. Our method generates clear deblurred images.

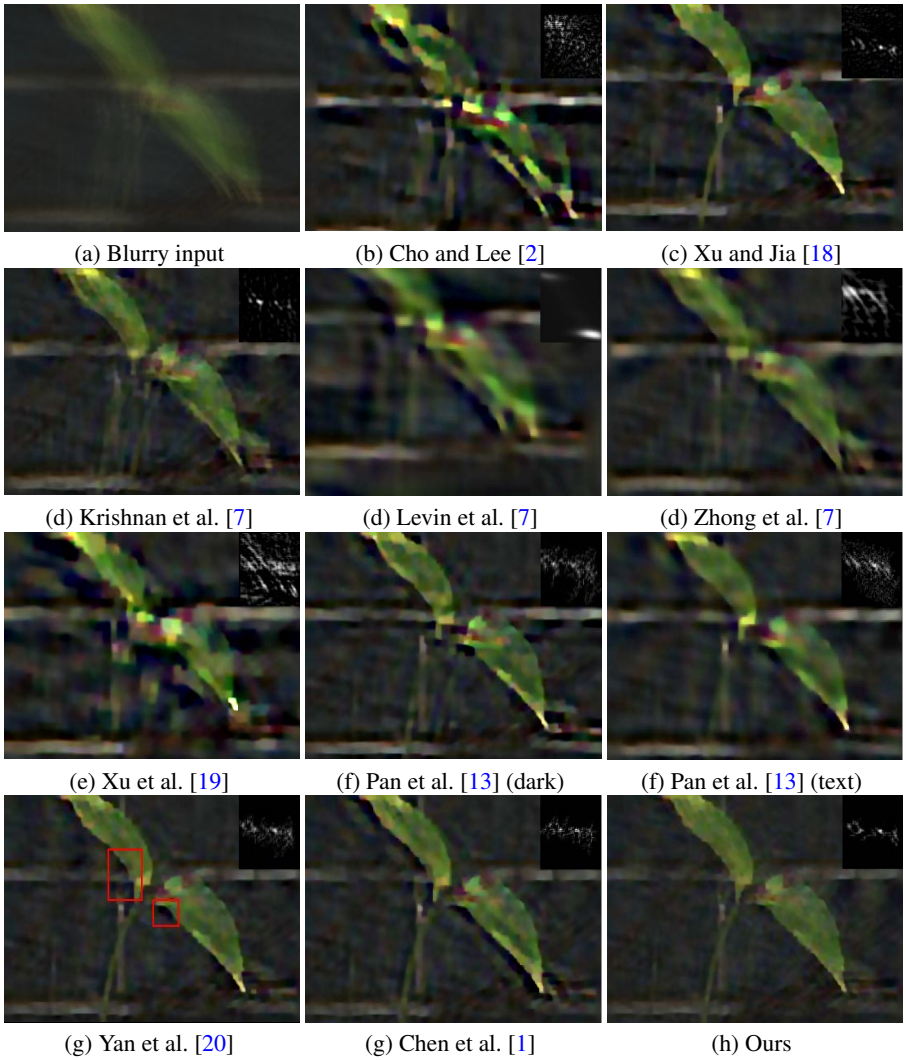

(a) Blurry input (b) Cho and Lee [2] (c) Xu and Jia [18]

(d) Krishnan et al. [7] (d) Levin et al. [7] (d) Zhong et al. [7]

(e) Xu et al. [19] (f) Pan et al. [13] (dark) (f) Pan et al. [13] (text)

(g) Yan et al. [20] (g) Chen et al. [1] (h) Ours

Fig. 4. Comparisons with state-of-the-art deblurring methods using real-world blur image. Here we use the same non-blid deconvolution method from [3] after the kernels are obtained. Our method generates clear deblurred images. Parts enclosed in the red boxes contain artifacts.

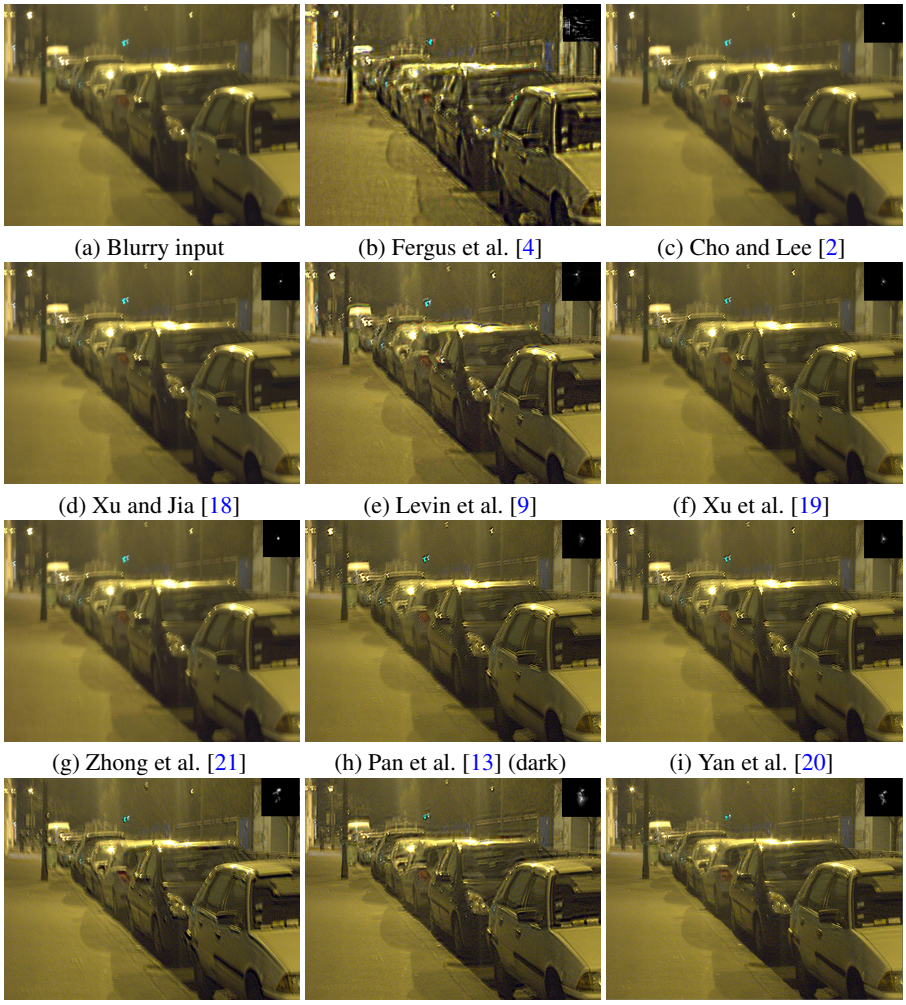

(a) Blurry input (b) Fergus et al. [4] (c) Cho and Lee [2]

(d) Xu and Jia [18] (e) Levin et al. [9] (f) Xu et al. [19]

(g) Zhong et al. [21] (h) Pan et al. [13] (dark) (i) Yan et al. [20]

(j) Hu et al. [5] (k) Pan et al. [12] (text) (l) Ours

Fig. 5. Comparisons with state-of-the-art deblurring methods using real-world blur image. Here we use the same non-blid deconvolution method from [16] after the kernels are obtained. When the image contains rich real-world noise, most state-of-the-art methods [2] [18] [19] [13] [20] fail to recover sharp image, while our method can still generate with sharp edges and clear details, which demonstrates the effectiveness of the proposed method in handling complicate noise situation.

(a) Blurry input (b) Cho and Lee [2] (c) Krishnan et al. [7]

(d) Xu et al. [19] (e) Pan et al. [13] (dark) (f) Yan et al. [20]

(g) Pan et al. [12] (text) (h) Hu et al. [5] (i) Ours

Fig. 6. Comparisons with state-of-the-art deblurring methods using real-world blur image. Here we use the same non-blid deconvolution method from [5] after the kernels are obtained. Note that several state-of-the-art methods [2] [7] [19]fail to estimate blur kernels due to the influence of saturated areas. Although the text deblurring method [12] and extream channel based methods [13] [20] are able to estimate blur kernels, the final deblurred image still contain blur effect as shown in the green boxes (Best viewed on high resolution with zoom-in). Compared to the low-light image deblurring method [5], our method generates comparable results both in the latent image and kernel.

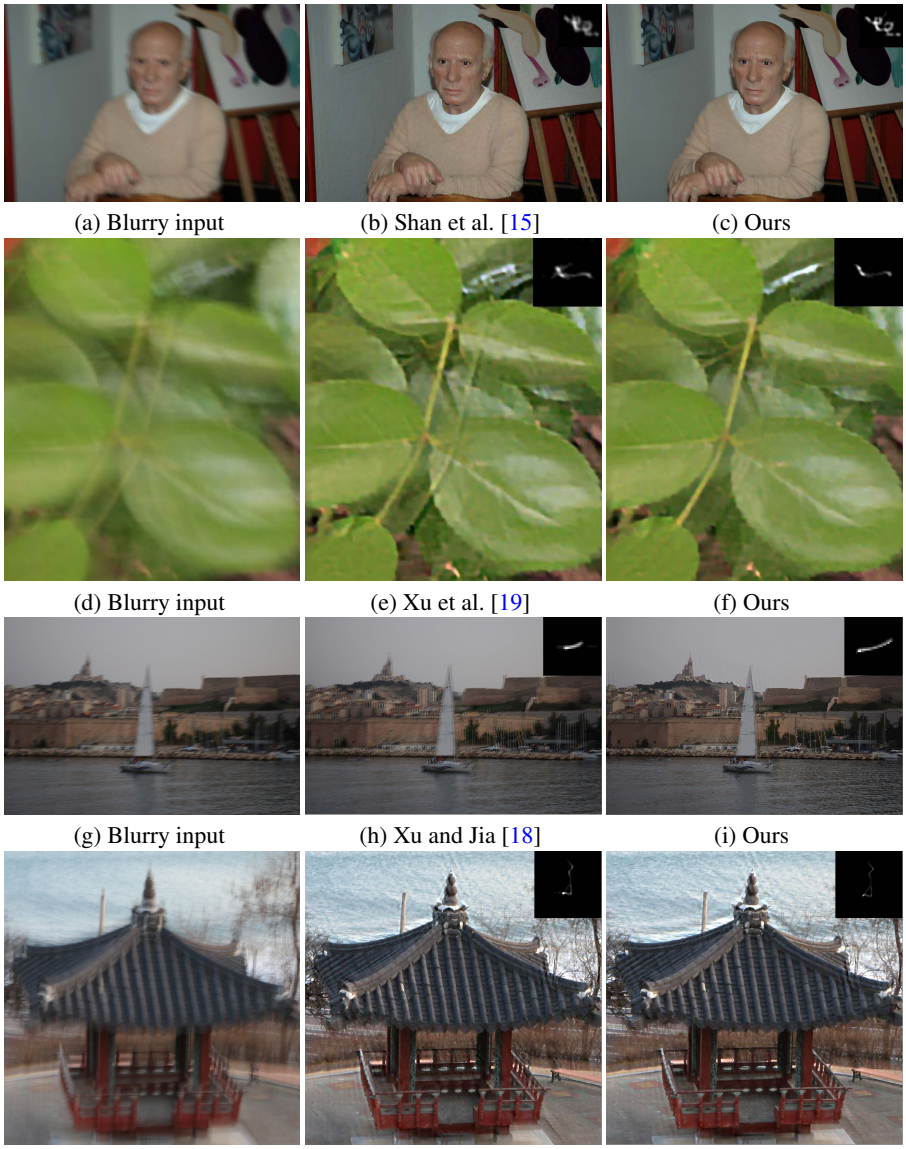

(a) Blurry input (b) Shan et al. [15] (c) Ours

(d) Blurry input (e) Xu et al. [19] (f) Ours

(g) Blurry input (h) Xu and Jia [18] (i) Ours

(j) Blurry input (k) Cho and Lee [2] (l) Ours

Fig. 7. Comparisons with state-of-the-art deblurring methods using their provided examples and reported results. Our method generates visually comparable or even better deblurring results.

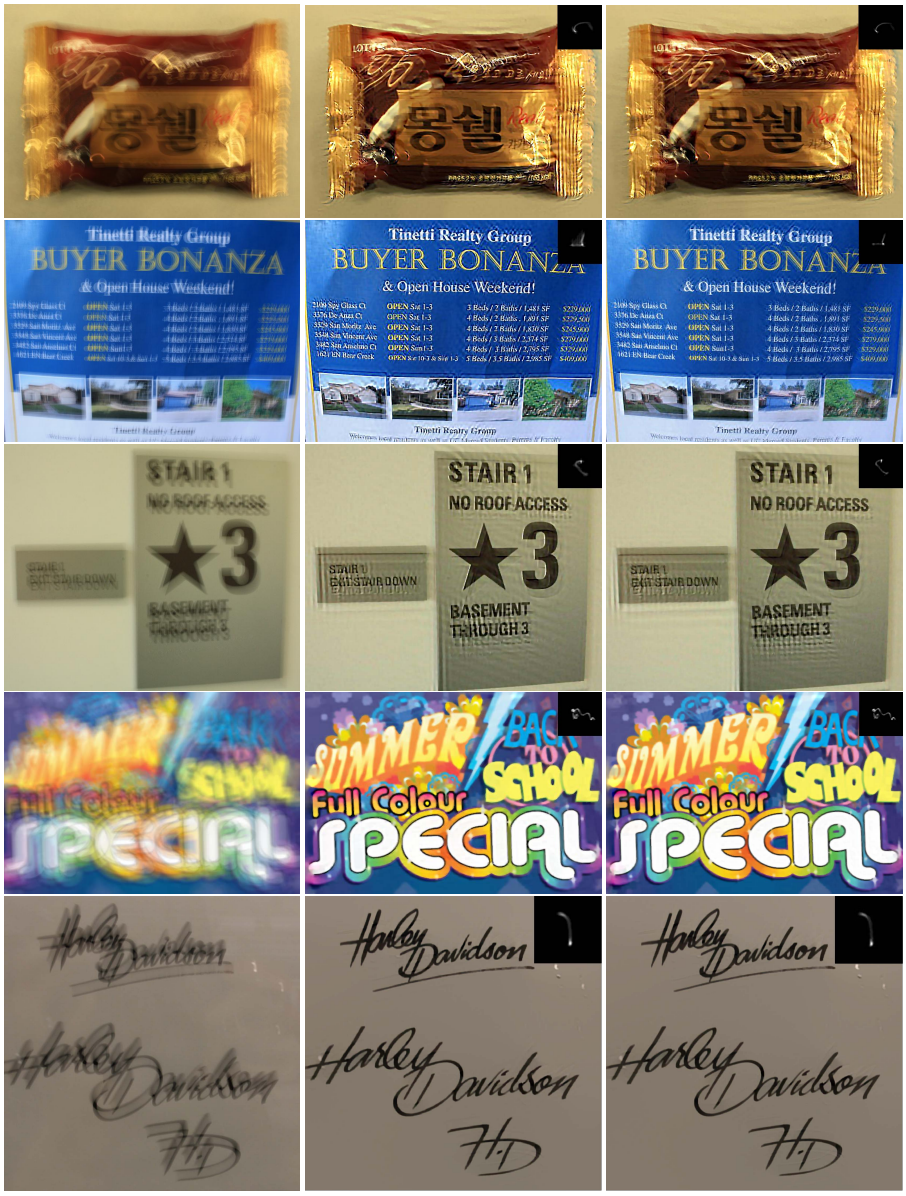

Blurry input Pan et al. [12] Ours

Fig. 8. Comparisons with state-of-the-art text deblurring method [12]. Our method generates visually comparable or even better deblurring results than the reported results in [12].

(a) Blurry input (b) Pan et al. [11] (c) Ours

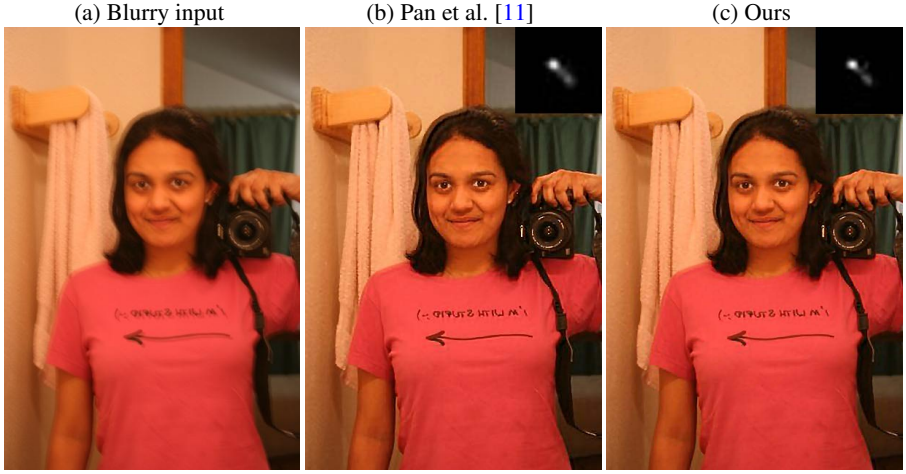

(a) Blurry input (b) Pan et al. [13] (c) Ours

Fig. 9. Comparisons with state-of-the-art methods on face blurred images. Our method generates comparable or even better deblurring results than state-of-the-art methods [11] [13].

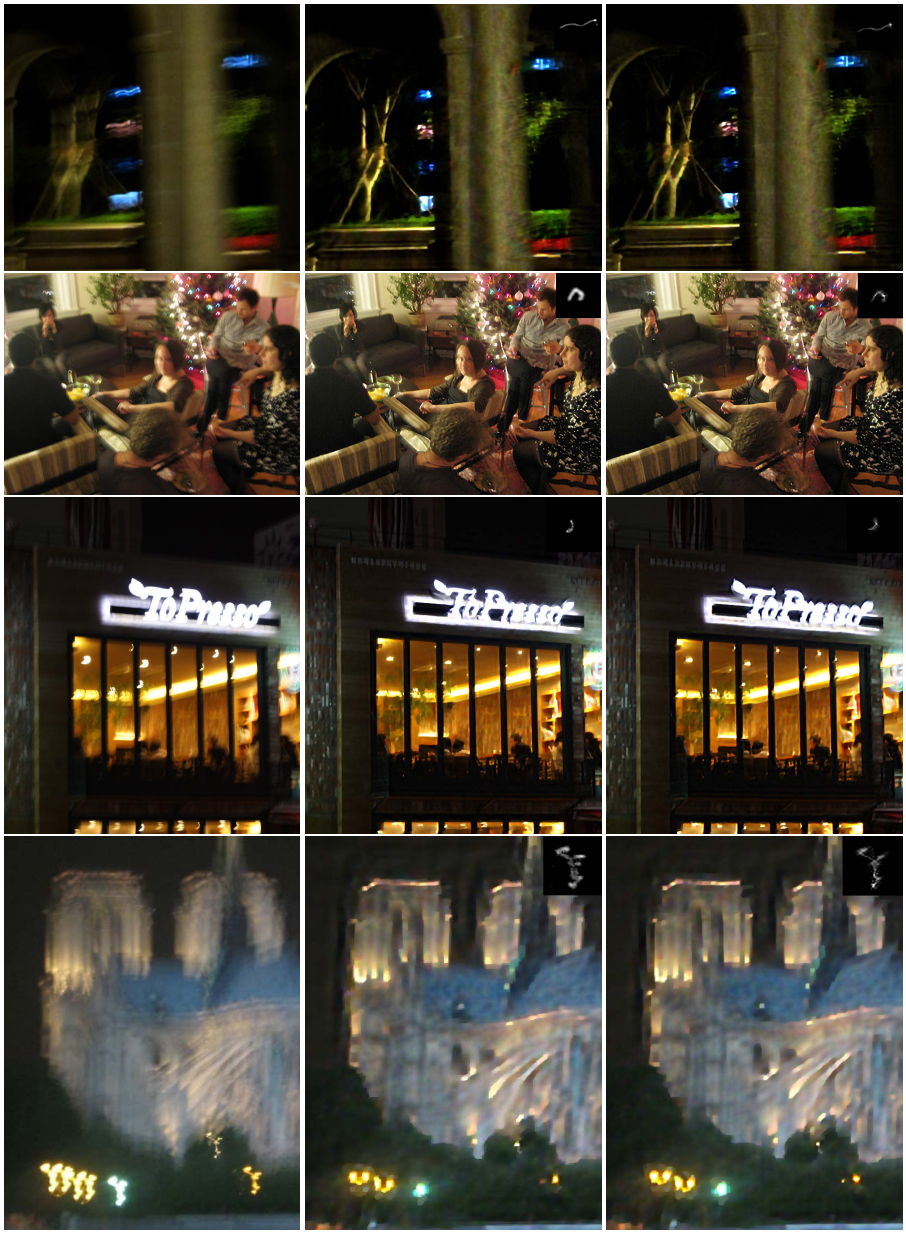

Blurry input Hu et al. [5] Ours

Fig. 10. Comparisons with state-of-the-art low-light image deblurring method [5]. Our method generates visually comparable or even better deblurring results than the reported results in [5].

References

1. Chen, L., Fang, F., Wang, T., Zhang, G.: Blind image deblurring with local maximum gradient prior. In: CVPR (2019)
2. Cho, S., Lee, S.: Fast motion deblurring. ACM T. Graphics **28**(5), 145 (2009)
3. Cho, T.S., Paris, S., Horn, B.K., Freeman, W.T.: Blur kernel estimation using the radon transform. In: CVPR (2011)
4. Fergus, R., Singh, B., Hertzmann, A., Roweis, S.T., Freeman, W.T.: Removing camera shake from a single photograph. ACM T. Graphics **25**(3), 787–794 (2006)
5. Hu, Z., Cho, S., Wang, J., Yang, M.H.: Deblurring low-light images with light streaks. In: CVPR (2014)
6. Köhler, R., Hirsch, M., Mohler, B., Schölkopf, B., Harmeling, S.: Recording and playback of camera shake: Benchmarking blind deconvolution with a real-world database. In: ECCV (2012)
7. Krishnan, D., Tay, T., Fergus, R.: Blind deconvolution using a normalized sparsity measure. In: CVPR (2011)
8. Levin, A., Weiss, Y., Durand, F., Freeman, W.T.: Understanding and evaluating blind deconvolution algorithms. In: CVPR (2009)
9. Levin, A., Weiss, Y., Durand, F., Freeman, W.T.: Efficient marginal likelihood optimization in blind deconvolution. In: CVPR (2011)
10. Michaeli, T., Irani, M.: Blind deblurring using internal patch recurrence. In: ECCV (2014)
11. Pan, J., Hu, Z., Su, Z., Yang, M.H.: Deblurring face images with exemplars. In: ECCV (2014)
12. Pan, J., Hu, Z., Su, Z., Yang, M.H.: l_0-regularized intensity and gradient prior for deblurring text images and beyond. IEEE TPAMI **39**(2), 342–355 (2017)
13. Pan, J., Sun, D., Pfister, H., Yang, M.H.: Blind image deblurring using dark channel prior. In: CVPR (2016)
14. Perrone, D., Favaro, P.: Total variation blind deconvolution: The devil is in the details. In: CVPR (2014)
15. Shan, Q., Jia, J., Agarwala, A.: High-quality motion deblurring from a single image. ACM T. Graphics **27**(3), 73 (2008)
16. Whyte, O., Sivic, J., Zisserman, A.: Deblurring shaken and partially saturated images. IJCV **110**(2), 185–201 (2014)
17. Xu, J., Li, H., Liang, Z., Zhang, D., Zhang, L.: Real-world noisy image denoising: A new benchmark. CoRR **abs/1804.02603** (2018)
18. Xu, L., Jia, J.: Two-phase kernel estimation for robust motion deblurring. In: ECCV (2010)
19. Xu, L., Zheng, S., Jia, J.: Unnatural l_0 sparse representation for natural image deblurring. In: CVPR (2013)
20. Yan, Y., Ren, W., Guo, Y., Wang, R., Cao, X.: Image deblurring via extreme channels prior. In: CVPR (2017)
21. Zhong, L., Cho, S., Metaxas, D., Paris, S., Wang, J.: Handling noise in single image deblurring using directional filters. In: CVPR (2013)